Renewable Energy 247 (2025) 123036

Contents lists available at ScienceDirect

Renewable Energy

journal homepage: www.elsevier.com/locate/renene

Enhancing low-frequency vibration energy harvesting using Negative Stiffness Inertial Amplifiers

Sudip Chowdhury [a],*, Sondipon Adhikari [a], Arnab Banerjee [b]

[a] Glasgow Computational Engineering Centre, James Watt School of Engineering, The University of Glasgow, Glasgow, Scotland, United Kingdom
[b] Civil Engineering Department, Indian Institute of Technology Delhi, India

ARTICLE INFO

Keywords:
Vibration energy harvesting
Negative stiffness inertial amplifiers
Piezoelectric energy harvester
Low-frequency energy harvesting
Optimisation

ABSTRACT

Conventional piezoelectric energy harvesters (PEHs) struggle to capture energy from low-frequency vibrations due to their intrinsic stiffness, limiting their applicability in real-world scenarios. The integration of Negative Stiffness Inertial Amplifiers (NSIAs) with cantilever bimorph PEHs enables a reduction in effective stiffness and amplification of dynamic mass, thereby enhancing low-frequency energy harvesting efficiency. A mathematical framework for NSIA-based energy harvesters is developed, analysing two circuit configurations (with and without an inductor). Key parameters, including stiffness ratio, mass ratio, and amplifier angle, are optimised. The harvested power is evaluated under both harmonic and random excitations. The proposed NSIA-integrated system achieves 99.97% higher power output compared to conventional harvesters. The inclusion of an inductor further enhances power generation at higher frequencies. Comparative analysis with traditional inertial amplifiers (IAs) shows that NSIAs outperform IAs by nearly two orders of magnitude. The findings demonstrate the transformative potential of NSIAs in vibration energy harvesting (VEH), offering a scalable and efficient solution for self-powered sensing, structural health monitoring, and industrial IoT applications.

1. Introduction

Vibration energy harvesting (VEH) has garnered significant attention as a promising approach for powering self-sustained wireless sensors [1], structural health monitoring (SHM) systems [2], and Internet of Things (IoT) applications [3]. By converting ambient mechanical vibrations into electrical energy, VEH offers an alternative to batteries, which suffer from limited lifespan and environmental concerns [4]. Among the various transduction mechanisms [5], piezoelectric energy harvesters (PEHs) have demonstrated superior energy density and ease of integration [6]. However, conventional PEHs exhibit fundamental limitations in low-frequency vibration energy harvesting [7]. Their high stiffness restricts operational bandwidth, making it difficult to capture energy efficiently from vibrations with long wavelengths and low amplitudes [8]. Additionally, low-frequency vibrations often suffer from weak excitation forces, leading to suboptimal strain generation in piezoelectric materials, which significantly limits power output [9]. The challenge is further compounded by the presence of damping effects and impedance mismatches, reducing the overall energy conversion efficiency in practical applications such as bridges, buildings, and industrial machinery [10]. Overcoming these difficulties requires innovative structural modifications that not only reduce effective stiffness but also amplify inertial effects, ensuring greater energy extraction from low-frequency vibrations [11]. Additionally, the integration of adaptive and tunable mechanisms is necessary to compensate for the inherent variability of environmental excitations, thereby enhancing low-frequency energy harvesting efficiency [12].

In recent years, several approaches have been proposed to improve low-frequency vibration energy harvesting (VEH) [13]. One common strategy involves frequency up-conversion using mechanical impact or nonlinear bi-stable mechanisms [14], which effectively convert low-frequency ambient vibrations into high-frequency oscillations for enhanced power generation [15]. These systems often incorporate magnetic or elastic elements to induce snap-through motion [16], thereby increasing energy extraction efficiency [17]. A novel dual-source vibration energy harvester (DVEH) has been introduced, which utilises a spherical pendulum to capture both flow-induced and multi-directional vibratory energies, broadening the range of operational frequencies [18]. While effective, these methods often introduce additional complexity, require external triggering, and may suffer from mechanical wear over extended operation [19]. Another widely explored approach is inertial amplification, where compliant mechanisms or resonant amplification structures, such as dynamic magnifiers and multi-degree-of-freedom (MDOF) systems, are employed to enhance

* Corresponding author.
E-mail address: Sudip.Chowdhury@glasgow.ac.uk (S. Chowdhury).

https://doi.org/10.1016/j.renene.2025.123036
Received 23 September 2024; Received in revised form 12 February 2025; Accepted 2 April 2025
Available online 10 April 2025

energy capture at low frequencies [20]. By leveraging resonant coupling between multiple masses, these configurations increase displacement responses, thereby improving power output [21]. However, such approaches typically necessitate precise tuning and additional mass, which may impose size and weight constraints [22]. Additionally, the presence of multiple resonances can introduce sensitivity to frequency shifts, reducing overall robustness [23]. To further extend the operational bandwidth and efficiency, researchers have explored the integration of nonlinear stiffness mechanisms into VEH designs [24]. In particular, negative stiffness mechanisms have gained significant attention as a promising solution to address these challenges [25]. By incorporating negative stiffness elements, the effective natural frequency of the system can be significantly reduced, enabling energy harvesting from ultra-low-frequency ambient vibrations [26]. Furthermore, negative stiffness elements [27], when integrated into piezoelectric energy harvesters (PEHs), have been shown to enhance power density by inducing large-amplitude oscillations even under weak excitation conditions [28]. Despite these advantages, existing implementations of negative stiffness VEH systems are often passive, relying on fixed structural configurations that lack adaptability to varying environmental conditions [29]. This limitation reduces their practical deployment in real-world scenarios where vibration characteristics fluctuate over time [30]. Additionally, some negative stiffness VEH designs exhibit bistable or multi-stable behaviour, which can lead to complex dynamic responses and inconsistent performance [31]. Active or tunable negative stiffness mechanisms have been proposed to overcome this limitation by allowing real-time adjustment of system parameters [32]. Such tunable designs leverage controllable electromagnetic or electromechanical actuators to dynamically modify the effective stiffness, thereby optimising energy harvesting performance across a wider frequency range [33]. However, these active configurations often require additional power consumption, which may offset the benefits of increased energy capture [34]. To achieve a balance between adaptability and energy efficiency, researchers are exploring hybrid strategies that integrate both passive and active tuning elements. Another emerging direction is the use of metamaterial-inspired architectures, which can tailor mechanical properties at the microscale to achieve desirable stiffness characteristics. These innovative designs aim to harness nonlinear interactions to further boost energy harvesting efficiency while maintaining a compact form factor. Overall, while significant progress has been made in enhancing low-frequency VEH, challenges remain in optimising system efficiency, scalability, and real-world applicability.

Despite these advancements, a significant gap remains in the development of a scalable and tunable negative stiffness mechanism that can substantially improve low-frequency VEH while maintaining structural simplicity and minimising additional weight [35]. Current studies primarily focus on single-degree-of-freedom (SDOF) designs with limited mass amplification effects, restricting their applicability to broadband, real-world environments [36]. Furthermore, most negative stiffness VEH solutions do not incorporate electrical circuit modifications that could further optimise energy extraction efficiency [37]. To bridge these gaps, a novel negative stiffness inertial amplifier (NSIA)-integrated PEH system is required, one that offers dynamic tunability, mass amplification, and enhanced power output at low frequencies.

This study introduces an innovative NSIA-integrated PEH system that addresses the limitations of conventional and existing negative stiffness VEH approaches. By leveraging NSIAs, a significant reduction in effective stiffness and a simultaneous amplification of the dynamic mass is achieved a significant reduction in effective stiffness and a simultaneous amplification of the dynamic mass, allowing for enhanced energy harvesting at ultra-low frequencies. Additionally, two circuit configurations, one without an inductor and another incorporating an inductor, are explored to assess their impact on harvested power under different excitation conditions. Optimisation of the proposed system is conducted through key parameters such as stiffness ratio, mass ratio, and amplifier angle to maximise energy conversion efficiency. The key contributions of this work are as follows:

- Development of a novel NSIA-integrated PEH system that significantly enhances low-frequency energy harvesting efficiency.
- Introduction of a tunable negative stiffness mechanism that dynamically reduces system stiffness and increases effective mass.
- Comparative evaluation of two circuit configurations, demonstrating the additional power enhancement potential of inductor-based designs.
- Mathematical formulation and parametric optimisation of the NSIA-PEH system under harmonic and random excitations.

By addressing the fundamental limitations of low-frequency VEH through NSIAs, this research introduces a novel method integrating a negative stiffness inertial amplifier with a cantilever bimorph piezoelectric energy harvester. The proposed system dynamically reduces stiffness while amplifying the effective mass, leading to enhanced power output at low frequencies. Two circuit configurations, one with and one without an inductor, are evaluated to optimise harvested energy under different excitation conditions. This research paves the way for the development of next-generation energy-harvesting technologies, with potential applications in SHM, IoT, and self-powered sensing networks. The remainder of this paper is structured as follows: Section 2 presents the theoretical framework and design principles of the NSIA-integrated PEH system. Section 3 details the mathematical modelling and optimisation strategies employed. Section 4 compares the performance of the proposed system with traditional inertial amplification-based harvesters. Section 5 concludes with key findings and future research directions.

2. Cantilever bimorph piezoelectric energy harvesters with negative stiffness inertial amplifiers

The negative stiffness inertial amplifiers provide dynamic negative stiffness and dynamic effective mass to the hosting structures. In this study, the hosting structure is considered as the cantilever bimorph piezoelectric energy harvesters, and the structural diagrams are shown in Fig. 1. The figure displays two distinct harvesting circuit configurations: subfigures Fig. 1(a) and (b) depict the circuits without an inductor and with one, respectively. The major mass of the harvester is its tip mass m, with two smaller masses m_a helping to provide inertial amplification. ϕ is the amplifier angle, and k_a is the amplifier stiffness. In the harvesting circuit, L is the inductor and R_l is the load resistance. The base-excitation $y_b(t)$ is the source of ambient energy. $y(t)$ and $v(t)$, respectively, represent the primary mass displacement and the voltage produced by the strain in the piezoelectric layers. $u(t) = y(t)\cos\phi/\sin\phi$ gives the horizontal velocity of the amplifier masses. Low amplitude vibration is applied to the fixed end of the cantilever beam. Consequently, the dynamic effective mass of the tip mass of the cantilever bimorph piezoelectric energy harvester is enhanced and simultaneously, the dynamic effective stiffness of the harvester is lowered by the negative stiffness inertial amplifier. First, the dynamic effective mass of the static mass of the amplifier, i.e. m_a, is increased by the laterally attached undamped spring-mass system [38] and expressed as

$$m_{ia} = \frac{m_d\left(\mu\,\omega^2 - \omega_b^2\right)}{\omega^2 - \omega_b^2} \tag{1}$$

where m_{ia} defines the dynamic effective mass of the amplifier. $\omega_b = \sqrt{k_b/m_b}$ defines the natural frequency of the lateral spring-mass system. $\mu = m_a/m_d$ defines the mass ratio of the negative stiffness inertial amplifier. The lateral spring-mass system provides dynamic effective negative stiffness to the harvester. m_d defines the total static mass of the negative stiffness inertial amplifier, i.e. $m_d = m_a + m_b$. m_b defines the static mass of the lateral spring-mass system and is derived as $m_b = (1-\mu)\,m_d$. m_{ia} is further written as

$$m_{ia} = \frac{m_d\left(\epsilon^2\mu - 1\right)}{\epsilon^2 - 1} \quad \text{or} \quad m_{ia} = \frac{m_d\left(\mu\,\eta^2 - \eta_b^2\right)}{\eta^2 - \eta_b^2} \tag{2}$$

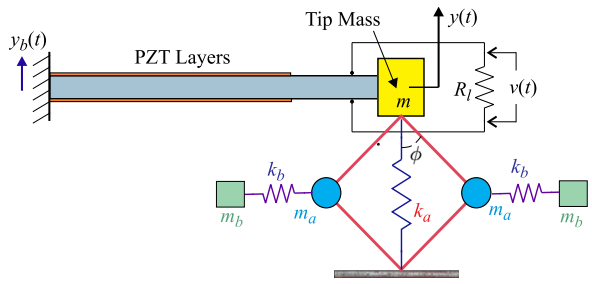

(a) Harvesting circuit without an inductor

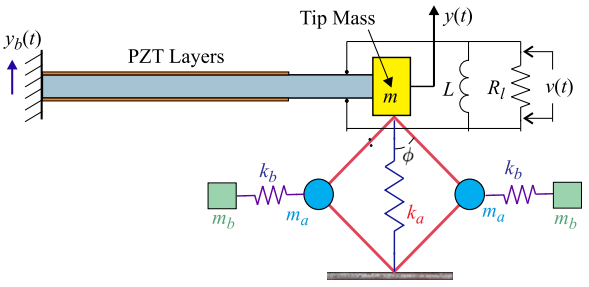

(b) Harvesting circuit with an inductor

Fig. 1. The structural configurations of the cantilever bimorph piezoelectric energy harvesters with negative stiffness inertial amplifiers. Two different configurations for the harvesting circuits are shown in the figure, namely, without and with an inductor are shown in subfigures (a) and (b) respectively. The tip mass m is the primary mass of the harvester, while two small masses m_a contribute towards the inertial amplification. The amplifier angle is ϕ and the amplifier stiffness is k_a. R_l is the load resistance and L is the inductor of the harvesting circuit. The source of the ambient energy is through the base-excitation $y_b(t)$. The displacement of the primary mass and the voltage generated due to the strain in the piezoelectric layers are denoted by $y(t)$ and $v(t)$ respectively. The horizontal velocity of the amplifier masses is given by $u(t) = y(t)\cos\phi/\sin\phi$.

where $\epsilon = \omega/\omega_b$, defines the excitation frequency ratio of the lateral spring-mass system. $\eta = \omega/\omega_n$ and $\eta_b = \omega_b/\omega_n$ define the excitation frequency ratio and frequency ratio of the lateral spring-mass system. ω_n defines the natural frequency of the harvester. Eq. (1) is added to the static mass of the tip mass of the harvester, i.e. m, and the dynamic effective mass of the harvester, i.e. m_h has been derived as

$$m_h = m + 0.5m_{ia}\left(1+\cot^2\phi\right) \tag{3}$$

Eq. (1) is substituted in Eq. (3).

$$\begin{aligned} m_h &= \frac{\omega^2\left(\Theta m_d\mu + m\right) - \omega_b^2\left(\Theta m_d + m\right)}{\omega^2 - \omega_b^2} \\ &= \frac{\eta^2\left(\Theta m_d\mu + m\right) - \eta_b^2\left(\Theta m_d + m\right)}{\eta^2 - \eta_b^2} \end{aligned} \tag{4}$$

where $\Theta = 0.5\left(1+\cot^2\phi\right)$.

3. Energy harvesting from harmonic base excitations

In the previous section the simplified equation of motion of a piezoelectric cantilever with inertial amplifier has been developed. Here, energy harvesting due to harmonic base motion applied to the system as ambient excitations is considered. Two cases of circuit configurations are considered.

3.1. Circuit without an inductor

A schematic diagram of a cantilever piezoelectric energy harvester with an inertial amplifier having a circuit without an inductor is shown in Fig. 2. Next, mathematical expressions for the harvested power and combinations of parameters that can maximise it are derived.

3.1.1. Quantification of the harvested power

Newton's second law is applied to derive the governing equations of motion of the cantilever bimorph piezoelectric energy harvesters with negative-stiffness inertial amplifier and expressed as

$$\begin{aligned} m_h\ddot{y}(t) + c_h\dot{y}(t) + \left(k_h + k_a\right)y(t) - \theta v(t) &= -m_h\ddot{y}_b(t) \\ C_p\dot{v}(t) + \frac{1}{R_l}v(t) + \theta\dot{y}(t) &= 0 \end{aligned} \tag{5}$$

where c_h and k_h define the dynamic effective damping and stiffness of the harvester, i.e $c_h = 2m_h\zeta_n\omega_n$ and $k_h = m_h\omega_n^2$. The dynamic effective mass of the negative stiffness inertial amplifier manipulates its stiffness, i.e. k_a and this k_a has been derived as $k_a = \Gamma_k k_h$. The stiffness ratio Γ_k in this case describes how stiff the spring k_a is in relation to the cantilever beam's stiffness in the first mode of vibration. To prevent excessive static strain on the beam, the spring k_a of the negative stiffness inertial amplifier should have sufficient strength to sustain the three masses' static weight. On the other hand, excessive spring stiffness will reduce captured power and cause little dynamic deformation. $y(t)$ represents the relative movement of the system in relation to the base excitation. $y_b(t)$ represents the voltage, $v(t)$ represents the voltage, R_l represents the load resistance, C_p represents the capacitance of the piezoelectric layer, t represents the time, and θ represents the electromechanical coupling. The coupled electromechanical behaviour of the energy harvester is considered in this study. The deterministic harmonic excitation $\ddot{y}_b(t) = Y_b e^{i\omega t}$ is applied at the fixed support of the cantilever and as a result, the steady-state responses of the cantilever beam are considered as

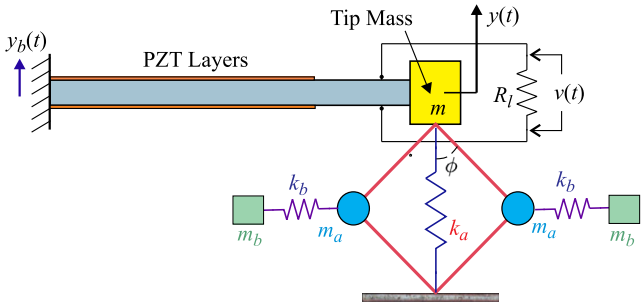

Fig. 2. A cantilever piezoelectric energy harvester with an inertial amplifier having a circuit without an inductor. R_l is the load resistance of the harvesting circuit. The source of the ambient energy is through the base-excitation $y_b(t)$. The displacement of the primary mass and the voltage generated due to the strain in the piezoelectric layers are denoted by $y(t)$ and $v(t)$ respectively.

$$y(t) = Ye^{i\omega t} \quad \text{and} \quad v(t) = Ve^{i\omega t} \tag{6}$$

In this context, ω represents the frequency of the driving force, whereas i denotes the imaginary unit $i = \sqrt{-1}$. By converting equations Eq. (5) into the frequency domain and dividing the first equation by m and the second equation by C_p, the following expressions are obtained:

$$\begin{aligned} \left(-\Gamma_h\omega^2 + 2i\omega\zeta_n\omega_n\Gamma_h + \left(1+\Gamma_k\right)\Gamma_h\omega_n^2\right)Y(i\omega) - \left(\frac{\theta}{m}\right)V(i\omega) &= -\Gamma_h Y_b \\ \left(i\omega + \frac{1}{R_l C_p}\right)V(i\omega) + \left(i\omega\frac{\theta}{C_p}\right)Y(i\omega) &= 0 \end{aligned} \tag{7}$$

Eq. (7) has been derived using the Laplace transformation [39]. The time-frequency conversion is essential for analysing the system's dynamic response in the frequency domain, enabling the identification of resonance behaviour and optimal energy harvesting conditions. This transformation allows for a more efficient evaluation of power output under varying excitation frequencies. $\Gamma_h = 1 + 0.5\mu_d\left(\frac{\mu\eta^2-\eta_b^2}{\eta^2-\eta_b^2}\right)\left(1+\cot^2\phi\right)$. $Y(i\omega)$ and $V(i\omega)$ represent the Fourier transforms of $y(t)$

and $v(t)$, respectively. Additionally, $\mu_d = m_d/m$, defines the ratio of the total static mass of the negative stiffness inertial amplifier to the static mass of the beam. This mass ratio is described in equation Eq. (7). The harvester's natural frequency (ω_n) and damping factor (ζ_n) are defined as follows:

$$\omega_n = \sqrt{\frac{k_h}{m_h}} \quad \text{and} \quad \zeta_n = \frac{c_h}{2m_h\omega_n} \tag{8}$$

Eq. (7) is divided by ω_n^2 and the transfer matrix is derived as

$$\begin{bmatrix} -\Gamma_h\eta^2 + 2i\eta\zeta_n\Gamma_h + \left(1+\Gamma_k\right)\Gamma_h & -\frac{\theta}{k} \\ i\eta\frac{\alpha\theta}{C_p} & (i\eta\alpha+1) \end{bmatrix} \begin{Bmatrix} Y(i\eta) \\ V(i\eta) \end{Bmatrix} = -\begin{Bmatrix} \Gamma_h \\ 0 \end{Bmatrix} \left(\frac{Y_b}{\omega_n^2}\right) \tag{9}$$

k defines the static stiffness of the harvester. The dimensionless frequency and time constant are defined as follows:

$$\eta = \frac{\omega}{\omega_n} \quad \text{and} \quad \alpha = \omega_n C_p R_l \tag{10}$$

It should be noted that α represents the time constant of the first-order electrical system, which has been made non-dimensional by employing the natural frequency of the mechanical system. The displacement and voltage in the frequency domain can be derived by inverting the coefficient matrix.

$$\begin{Bmatrix} Y(i\eta) \\ V(i\eta) \end{Bmatrix} = -\frac{1}{\Delta_1(i\eta)} \begin{bmatrix} (i\eta\alpha+1) & \frac{\theta}{k} \\ -i\eta\frac{\alpha\theta}{C_p} & -\Gamma_h\eta^2 + 2i\eta\zeta_n\Gamma_h + \left(1+\Gamma_k\right)\Gamma_h \end{bmatrix} \times \begin{Bmatrix} \Gamma_h \\ 0 \end{Bmatrix} \left(\frac{Y_b}{\omega_n^2}\right) \tag{11}$$

The determinant of the coefficient matrix is calculated using the equation shown above.

$$\begin{aligned} \Delta_1(i\eta) = {} & \left(0.5\alpha\mu\mu_d + \alpha + 0.5\left(\cot^2(\phi)\right)\alpha\mu\mu_d\right)(i\eta)^5 \\ & + \begin{pmatrix} \alpha\mu\mu_d\zeta_n + 0.5\mu\mu_d + 2.0\alpha\zeta_n + 1 \\ +0.5\left(\cot^2(\phi)\right)\mu\mu_d + \left(\cot^2(\phi)\right)\alpha\mu\mu_d\zeta_n \end{pmatrix}(i\eta)^4 \\ & + \begin{pmatrix} 2.0\zeta_n + \alpha\eta_b^2 + \alpha\mu_k + 0.5\alpha\mu\mu_d\mu_k \\ +0.5\alpha\mu\mu_d + 0.5\alpha\eta_b^2\mu_d + \mu\mu_d\zeta_n + \alpha\kappa^2 \\ +\alpha + \left(\cot^2(\phi)\right)\mu\mu_d\zeta_n + 0.5\left(\cot^2(\phi)\right)\alpha\mu\mu_d \\ +0.5\left(\cot^2(\phi)\right)\alpha\mu\mu_d\mu_k + 0.5\left(\cot^2(\phi)\right)\alpha\eta_b^2\mu_d \end{pmatrix}(i\eta)^3 \\ & + \begin{pmatrix} 2.0\alpha\eta_b^2\zeta_n + \mu_k + \eta_b^2 + 0.5\mu_d\eta_b^2 \\ +0.5\mu\mu_d + \alpha\eta_b^2\mu_d\zeta_n + 1.0 + 0.5\mu_d\eta_b^2\left(\cot^2(\phi)\right) \\ +0.5\left(\cot^2(\phi)\right)\mu\mu_d + \left(\cot^2(\phi)\right)\alpha\eta_b^2\mu_d\zeta_n \\ +0.5\mu\mu_d\mu_k + 0.5\left(\cot^2(\phi)\right)\mu\mu_d\mu_k \end{pmatrix}(i\eta)^2 \\ & + \begin{pmatrix} 2.0\eta_b^2\zeta_n + \alpha\eta_b^2 + \alpha\eta_b^2\mu_k \\ +0.5\alpha\eta_b^2\mu_d\mu_k + 0.5\left(\cot^2(\phi)\right)\alpha\eta_b^2\mu_d\mu_k \\ +\eta_b^2\mu_d\zeta_n + \alpha\eta_b^2\kappa^2 + \mu_d\eta_b^2\left(\cot^2(\phi)\right)\zeta_n \\ +0.5\alpha\eta_b^2\mu_d + 0.5\left(\cot^2(\phi)\right)\alpha\eta_b^2\mu_d \\ +0.5\mu_d\eta_b^2 + \eta_b^2\mu_k + 0.5\eta_b^2\mu_d\mu_k + \eta_b^2 \\ +0.5\left(\cot^2(\phi)\right)\eta_b^2\mu_d\mu_k + 0.5\mu_d\eta_b^2\left(\cot^2(\phi)\right) \end{pmatrix}(i\eta) \end{aligned} \tag{12}$$

The non-dimensional electromechanical coupling coefficient is a parameter that is defined as

$$\kappa^2 = \frac{\theta^2}{kC_p} \tag{13}$$

By solving equation Eq. (11), the dynamic response and the voltage output of the system caused by the harmonic base excitation can be determined.

$$Y(i\eta) = \frac{(-i\eta\alpha - 1)\left(0.5\mu_d\eta_b^2\left(\csc^2(\phi)\right) - 0.5\mu_d\mu\eta^2\left(\csc^2(\phi)\right) + \eta_b^2 - \eta^2\right)}{\Delta_1(i\eta)} \times \left(\frac{Y_b}{\omega_n^2}\right) \tag{14}$$

$$V(i\eta) = \frac{i\eta\alpha\theta\left(0.5\mu_d\eta_b^2\left(\csc^2(\phi)\right) - 0.5\mu_d\mu\eta^2\left(\csc^2(\phi)\right) + \eta_b^2 - \eta^2\right)}{C_p\Delta_1(i\eta)}\left(\frac{Y_b}{\omega_n^2}\right) \tag{15}$$

It is advantageous to observe the response quantities in a dimensionless form. The electricity obtained from the harvest is determined by

$$P(\eta) = \frac{V^2(\eta)}{R_l} \tag{16}$$

Since R_l remains constant, in order to describe power in a non-dimensional form, it is just necessary to non-dimensionalise the voltage. There are multiple methods to accomplish this. To simplify the analysis, the voltage at $\eta = 1$ is used as a reference point for normalisation, assuming zero damping and the absence of the inertial amplifier.

$$V_0 = V(i\eta)|_{\{\eta=1,\zeta_n=0,\mu_d=0,\Gamma_k=0\}} = \frac{\theta}{\kappa^2 C_p}\left(\frac{Y_b}{\omega_n^2}\right) \tag{17}$$

By utilising this method, the voltage response is derived in a non-dimensional form.

$$\hat{V}(i\eta) = \frac{V(i\eta)}{V_0} = \frac{i\eta\kappa^2\alpha\left(0.5\mu_d\eta_b^2\left(\csc^2(\phi)\right) - 0.5\mu_d\mu\eta^2\left(\csc^2(\phi)\right) + \eta_b^2 - \eta^2\right)}{\Delta_1(i\eta)} \tag{18}$$

The dimensionless power is thus expressed as

$$\hat{P}(\eta) = \frac{P(\eta)}{P_0} = \left|\frac{V(i\eta)}{V_0}\right|^2 = \left|\hat{V}(i\eta)\right|^2 \tag{19}$$

In the context of harmonic base excitation, a primary focus is the fluctuation of harvested power as a function of the driving frequency of the base excitation. To acquire physical insights, the results obtained thus far are applied numerically to a specific example problem. Table 1 presents the system parameters for the simulations, as sourced from Ref. [40]. For these parameter values, $V_0 = 896.87$ V is derived when $Y_b = 1$ mm, with the negative sign neglected. The value of V_0 will vary considerably based on the system parameters. The results of this study are presented in a non-dimensional format for the sake of generality. The actual values can be derived by multiplying the respective normalisation factors. Fig. 3 illustrates the non-dimensional power response of a cantilever piezoelectric energy harvester equipped with an inertial amplifier, plotted against non-dimensional frequency. This figure contrasts the performance of two different inertial amplifier configurations with that of a traditional harvester lacking an inertial amplifier. The primary emphasis of the figure is to demonstrate the improved power harvesting efficiency of the proposed systems, especially at lower frequencies, in contrast to traditional systems. The data indicates that the proposed systems with inertial amplifiers substantially exceed the classical harvester in power output, especially at lower frequencies. The configuration shown in Fig. 3(a) (where $\mu_d = 0.2$ and $\phi = 10°$) achieves a 96.27% power enhancement compared to the traditional harvester. The maximum non-dimensional power generated by NSIA is 25.0727, whereas the traditional harvester without NSIA produces a power output of 0.9334. For instance, the system depicted in Fig. 3(b), with parameters $\mu_d = 1$, and $\phi = 15°$, exhibits a power output exceeding 98.63% that of the traditional harvester at lower frequencies. The maximum non-dimensional power generated by NSIA is 68.6218, whereas the traditional harvester without NSIA produces a power output of 0.9334. These results highlight the significant power enhancement achieved through NSIA, demonstrating its effectiveness in improving energy harvesting performance across different configurations. The maximum power output from each harvester is listed in Table 2. Fig. 4 illustrates the non-dimensional power response of a cantilever

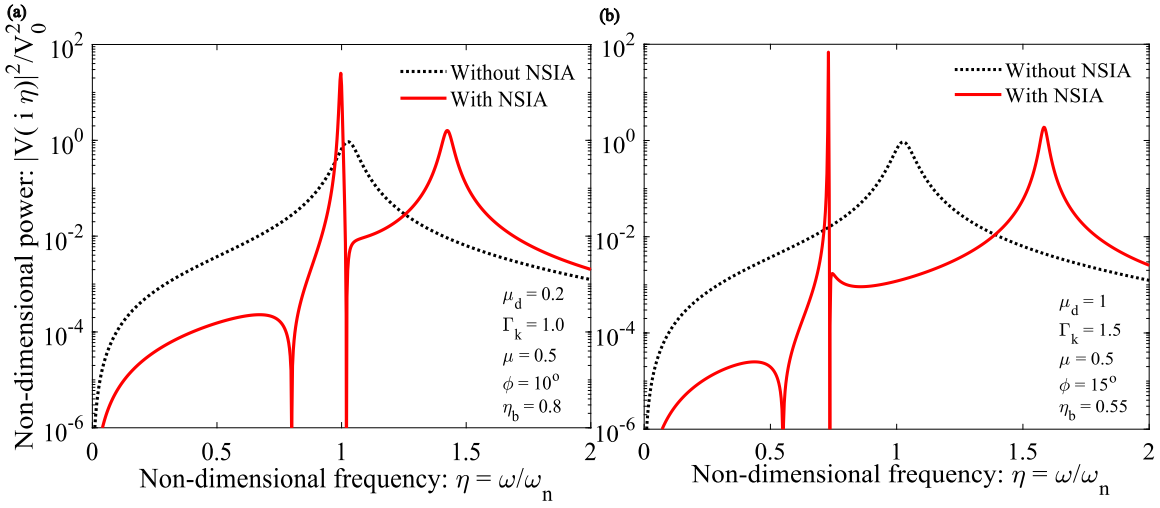

Fig. 3. The non-dimensional power of a harvester devoid of an inductor as a function of non-dimensional frequency. The powers derived from the classical harvester lacking an inertial amplifier and the proposed harvester featuring two distinct inertial amplifier configurations are presented for comparison. The power generated by the proposed harvesters is 96.27% and 98.63% superior to the conventional harvester.

Table 1
Parameter values used in the simulation [40].

Parameter	Value	Unit
m	9.12×10^{-3}	kg
k	4.1×10^3	N/m
c	0.135	Ns/m
R_l	3×10^4	Ohm
C_p	4.3×10^{-8}	F
θ	-4.57×10^{-3}	N/V
ζ_n	0.011	–
α	0.8649	–
κ^2	0.1185	–

Table 2
Non-dimensional power under harmonic excitation.

Device	Power
NSIA ($\phi = 10°$)	25.0727
NSIA ($\phi = 15°$)	68.6218
Without NSIA (Conventional energy harvester)	0.9334

Table 3
Non-dimensional power under random excitation.

Device	Power
NSIA ($\phi = 10°$)	1.406×10^{13} dB/Hz
NSIA ($\phi = 15°$)	8.244×10^{13} dB/Hz
Without NSIA (Conventional energy harvester)	2.0985×10^{10} dB/Hz

piezoelectric energy harvester equipped with an inertial amplifier under random excitation, plotted against non-dimensional frequency. This figure compares the performance of two different inertial amplifier configurations with that of a traditional harvester without an inertial amplifier. The primary objective is to highlight the enhanced power harvesting capability of the proposed systems, particularly in response to broadband random excitation, as opposed to traditional systems. The results indicate that the proposed systems with inertial amplifiers significantly outperform the conventional harvester, particularly at lower frequencies. For instance, the configuration shown in Fig. 3(a) (where $\mu_d = 0.2$ and $\phi = 10°$) achieves a 99.85% increase in power output compared to the traditional harvester. Under random excitation, the maximum non-dimensional power generated by NSIA is 1.406×10^{13} dB/Hz, whereas the traditional harvester without NSIA produces only 2.0985×10^{10} dB/Hz. Similarly, the system depicted in Fig. 3(b), with parameters $\mu_d = 1$ and $\phi = 15°$, exhibits a power enhancement exceeding 99.97% over the traditional harvester at lower frequencies. The maximum non-dimensional power attained by NSIA in this case is 8.244×10^{13} dB/Hz, in contrast to 2.245×10^{10} dB/Hz for the traditional system. These findings underscore the substantial power enhancement achieved by NSIA under random excitation, demonstrating its efficacy in optimising energy harvesting performance across diverse configurations. The maximum power output from each harvester is listed in Table 3.

3.1.2. Optimisation of the harvested power

The initial step to optimise the harvested power is to identify the frequency at which the power maxima occur. In lightly damped systems devoid of the inertial amplifier, the harvested power reaches its maximum at approximately $\eta \approx 1$. To determine the frequency at which the harvested power reaches its maximum, the derivative of the normalised power, as specified in equation Eq. (19), with respect to the normalised frequency squared, is set to zero.

$$\frac{\partial \hat{P}(\eta^2)}{\partial \eta^2} = 0 \tag{20}$$

By simplifying this, the requisite condition is derived as:

$$\left(-0.125\left(\sin^2(\phi)\right) - 0.0625\mu\mu_d\right)\eta_{max}^2 + 0.125\left(\sin^2(\phi)\right)\eta_b^2 + 0.0625\mu_d\eta_b^2 = 0$$

$$\eta_{max}^2 = \frac{\eta_b^2\left(2\left(\sin^2(\phi)\right) + \mu_d\right)}{\mu\mu_d + 2\left(\sin^2(\phi)\right)} \tag{21}$$

The maximum harvested power's non-dimensional frequency is consequently determined by the inertial amplifier parameters, time constant, and electromechanical coupling coefficient.

The non-dimensional power of two distinct inertial amplifiers is illustrated in Fig. 5. Four values of the damping factors for the energy harvesters have been evaluated. Their range extends from undamped to a damping factor of 10%. As anticipated, reduced damping in the harvester results in increased power extraction from the harmonic base excitation. The value of $\eta_{\max}$ derived from equation Eq. (21) is indicated in Fig. 5 by an asterisk ('*'). It closely aligns with the frequency at which the harvested power is maximised for all four damping values. The non-dimensional frequencies for the maximum power derived from Eq. (21) are 1.01 and 0.73, respectively. Upon comparison with the precise results, it was confirmed that for all damping values, the frequency corresponding to maximum power remains significantly unchanged. It

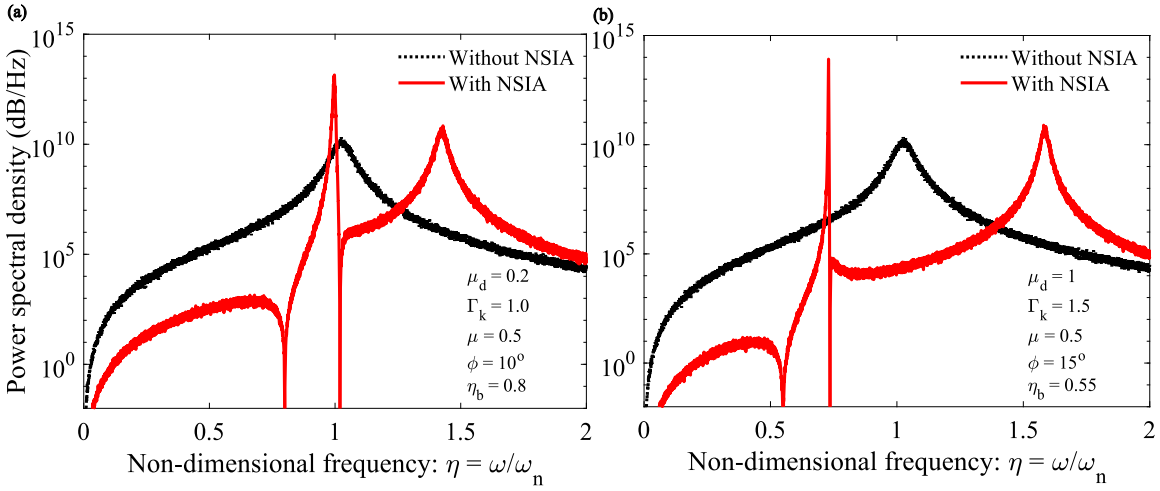

Fig. 4. The non-dimensional power of a harvester devoid of an inductor as a function of non-dimensional frequency. The harvester is subjected to random excitation. The powers derived from the classical harvester lacking an inertial amplifier and the proposed harvester featuring two distinct inertial amplifier configurations are presented for comparison. The power generated by the proposed harvesters is 99.85% and 99.97% superior to the conventional harvester.

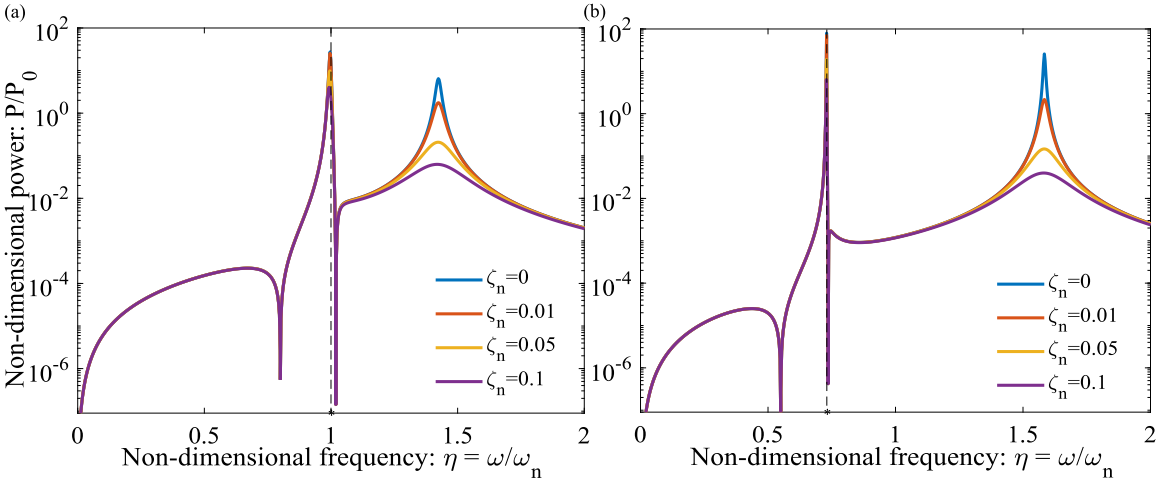

Fig. 5. The non-dimensional power of a harvester devoid of an inductor ($\alpha = 0.8649$, $\kappa^2 = 0.1185$) as a function of the non-dimensional frequency for five chosen values of damping factors. The frequency of maximum power (η_{max}) derived from equation Eq. (21) is indicated by a '*' in Fig. 5. Four of the damping factors for the energy harvesters have been examined for demonstration purposes.

is important to observe that in both instances, this value is considerably lower than that of the classical harvester lacking an inertial amplifier, for which η_{max} approaches 1.03. This unequivocally illustrates that the optimal power is extracted at a lower frequency in comparison to the traditional harvester. For Fig. 5(a), the maximum power outputs evaluated for $\zeta_n = 0, 0.01, 0.05$, and 0.10 are 27.4627, 25.4546, 9.8303, and 4.0384, respectively. For Fig. 5(b), the maximum power outputs evaluated for $\zeta_n = 0, 0.01, 0.05$, and 0.10 are 79.7691, 70.3275, 19.0902, and 6.3878, respectively. The increment in the harvester's damping ratio reduces its power generation capacity. Therefore, a lower damping ratio is preferable for maximising the energy harvesting performance. Fig. 6 presents the non-dimensional power spectral density (PSD) response of a harvester under random excitation, with results shown for four selected damping factor values ($\zeta_n = 0, 0.01, 0.05, 0.10$). The analysis is split into two cases: (a) parameters $\mu_a = 0.2$, $\Gamma_k = 1$, $\mu = 0.5$, $\phi_b = 10°$, and $\eta_b = 0.8$, and (b) parameters $\mu_a = 1.5$, $\Gamma_k = 1.0$, $\mu = 0.5$, $\phi_b = 15°$, and $\eta_b = 0.55$. Fig. 6(a): This configuration demonstrates the harvester's response with a smaller mass ratio and lower excitation frequency parameter:

- Resonance peaks: The PSD exhibits sharp peaks near $\eta = 1$, corresponding to the harvester's resonance frequency. The sharpness and amplitude of these peaks are most prominent for $\zeta_n = 0$ and decrease with increasing damping.
- Damping effects: As ζ_n increases from 0 to 0.10, the resonance peaks broaden and flatten, indicating reduced energy harvesting efficiency. The maximum power is achieved at lower damping, showing the critical role of minimising damping for high power generation.
- Low-frequency behaviour: At lower frequencies ($\eta < 0.5$), the PSD is negligible, indicating the harvester's inefficiency in capturing energy away from resonance under these conditions.

Fig. 6(b): This configuration explores the harvester's response with a larger mass ratio and higher excitation frequency parameter:

- Resonance peaks: The resonance peaks are sharper and higher than in (a), reflecting the enhanced energy harvesting capability due to increased dynamic mass and altered system stiffness.
- Damping effects: Similar to Fig. 6(a), higher damping flattens the peaks and reduces the harvester's overall efficiency. However, due to the larger mass ratio, the harvester shows improved resilience to damping, maintaining relatively higher PSD levels for $\zeta_n = 0.01$ compared to Fig. 6(a).

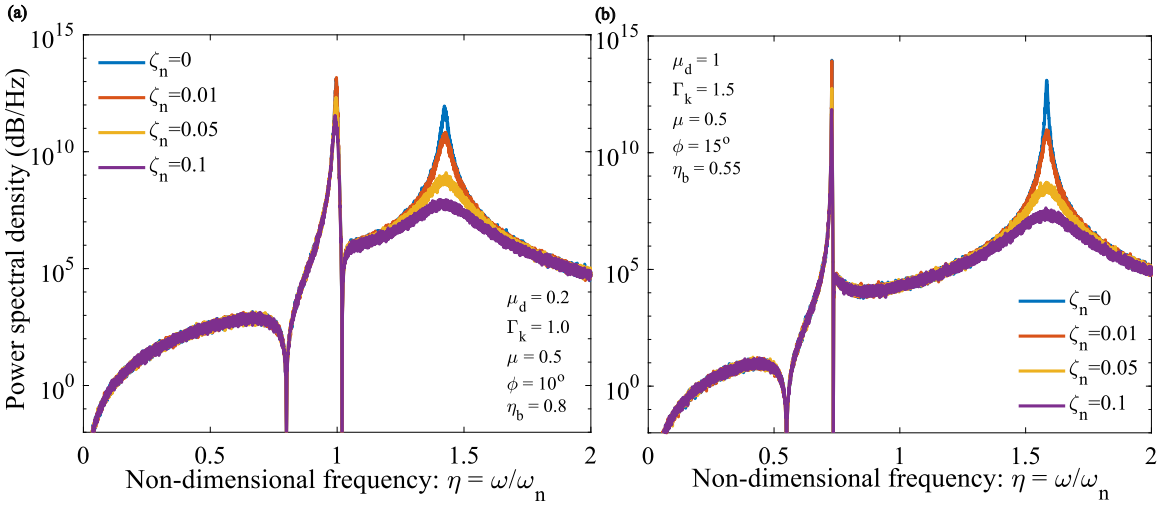

Fig. 6. The non-dimensional power response of a harvester without an inductor ($\alpha = 0.8649$, $\kappa^2 = 0.1185$) under random excitation, plotted as a function of the non-dimensional frequency for four selected damping factor values. Four specific damping factor values have been analysed to demonstrate their influence on energy harvesting performance.

- Low-frequency behaviour: The PSD at lower frequencies ($\eta < 0.5$) is slightly improved compared to Fig. 6(a), attributed to the increased dynamic mass and lower effective stiffness provided by the altered parameters.

Comparison of Fig. 6(a) and Fig. 6(b): Parameter Influence: The configuration in Fig. 6(b) exhibits superior performance due to the higher mass ratio and dynamic amplification effects, enabling better energy harvesting even at moderate damping levels.

- Resonance behaviour: Both cases show that minimising damping is critical for maximising resonance-based energy harvesting, but configuration Fig. 6(b) offers a broader operational range and higher peak PSD values.
- Low-frequency harvesting: While both cases perform poorly at low frequencies, configuration Fig. 6(b) shows slight improvement due to better dynamic tuning. The figures emphasise the critical role of system parameters such as mass ratio, damping, and stiffness in optimising the harvester's performance.

Configuration Fig. 6(b) demonstrates the potential for enhancing energy harvesting by increasing dynamic mass and fine-tuning stiffness, highlighting the importance of careful parameter selection. Overall, minimising damping remains crucial for maximising energy harvesting efficiency, particularly under random excitations.

3.2. Circuit with an inductor

A schematic representation of a cantilever piezoelectric energy harvester featuring an inertial amplifier and a circuit containing an inductor is illustrated in Fig. 7. Subsequently, mathematical expressions for the harvested power are formulated, and parameter combinations that can optimise it are identified.

3.2.1. Quantification of the harvested power

The piezoelectric vibration energy harvester, which includes a circuit with an inductor, is illustrated in Fig. 7. In this instance, the electrical equation is formulated as

$$C_p\ddot{v}(t) + \frac{1}{R_l}\dot{v}(t) + \frac{1}{L}v(t) + \theta\ddot{y}(t) = 0 \tag{22}$$

where L is the inductance of the circuit. By converting equation Eq. (22) into the frequency domain and dividing by $C_p\omega_n^2$, one obtains

$$-\eta^2\frac{\theta}{C_p}Y(\mathrm{i}\eta) + \left(-\eta^2 + \mathrm{i}\eta\frac{1}{\alpha} + \frac{1}{\beta}\right)V(\mathrm{i}\eta) = 0 \tag{23}$$

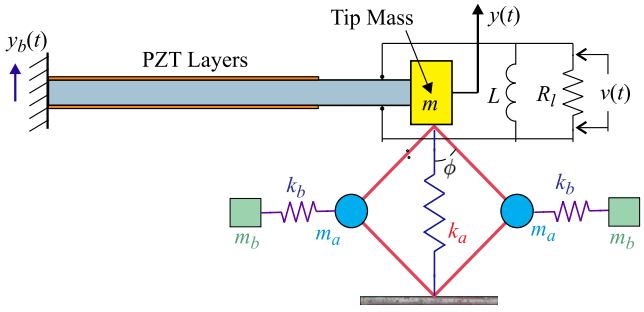

Fig. 7. A cantilever piezoelectric energy harvester equipped with an inertial amplifier and a circuit containing an inductor. R_l denotes the load resistance, while L represents the inductor within the harvesting circuit. The origin of the ambient energy is via the base excitation $y_b(t)$. The primary mass's displacement and the voltage produced from the strain in the piezoelectric layers are represented by $y(t)$ and $v(t)$, respectively.

where the normalised inductor parameter is defined as

$$\beta = \omega_n^2 LC_p \tag{24}$$

It represents the ratio of mechanical to electrical natural frequencies. The governing equation of motion of the negative stiffness inertially amplified piezoelectric energy harvester is derived as

$$m_h\ddot{y}(t) + c_h\dot{y}(t) + \left(k_h + k_a\right)y(t) - \theta v(t) = -m_h\ddot{y}_b(t) \tag{25}$$

The frequency response function has been derived using the considered steady-state responses in Eq. (25) and Eq. (22) and expressed as

$$\begin{bmatrix} -\Gamma_h\eta^2 + 2\mathrm{i}\eta\zeta_n\Gamma_h + \left(1+\Gamma_k\right)\Gamma_h & -\frac{\theta}{k} \\ -\eta^2\frac{\alpha\beta\theta}{C_p} & \alpha\left(1-\beta\eta^2\right) + \mathrm{i}\eta\beta \end{bmatrix} \begin{Bmatrix} Y(\mathrm{i}\eta) \\ V(\mathrm{i}\eta) \end{Bmatrix} = -\begin{Bmatrix} \Gamma_h \\ 0 \end{Bmatrix}\left(\frac{Y_b}{\omega_n^2}\right) \tag{26}$$

Eq. (26) has been derived using the Laplace transformation [39]. The time-frequency conversion is essential for analysing the system's dynamic response in the frequency domain, enabling the identification of resonance behaviour and optimal energy harvesting conditions. This transformation allows for a more efficient evaluation of power output under varying excitation frequencies. k defines the static stiffness of the harvester. The displacement and voltage in the frequency domain can

be obtained by inverting the coefficient matrix.

$$\begin{Bmatrix} Y(i\eta) \\ V(i\eta) \end{Bmatrix} = -\frac{1}{\Delta_2(i\eta)} \begin{bmatrix} \alpha\left(1-\beta\eta^2\right)+i\eta\beta & \frac{\theta}{k} \\ \eta^2 \frac{\alpha\beta\theta}{C_p} & -\Gamma_h\eta^2+2i\eta\zeta_n\Gamma_h+\left(1+\Gamma_k\right)\Gamma_h \end{bmatrix} \times \begin{Bmatrix} \Gamma_h \\ 0 \end{Bmatrix} \left(\frac{Y_b}{\omega_n^2}\right) \tag{27}$$

where the determinant of the coefficient matrix exists

$$\begin{aligned} \Delta_2(i\eta) = & \left(\alpha\beta+0.5\alpha\beta\mu\mu_d\left(\csc^2(\phi)\right)\right)(i\eta)^6 \\ & +\left(0.5\beta\mu\mu_d\left(\csc^2(\phi)\right)+\alpha\beta\mu\mu_d\zeta_n\left(\csc^2(\phi)\right)+\beta+2.0\alpha\beta\zeta_n\right)(i\eta)^5 \\ & +\begin{pmatrix} 0.5\alpha\mu\mu_d\left(\csc^2(\phi)\right)+0.5\alpha\beta\mu\mu_d\mu_k\left(\csc^2(\phi)\right)+1.0\alpha\beta \\ +1.0\alpha+\alpha\beta\kappa^2+\alpha\beta\mu_k+2\beta\zeta_n+\beta\mu\mu_d\zeta_n\left(\csc^2(\phi)\right) \\ +\alpha\beta\eta_b^2+0.5\alpha\beta\mu\mu_d\left(\csc^2(\phi)\right)+0.5\alpha\beta\eta_b^2\mu_d\left(\csc^2(\phi)\right) \end{pmatrix}(i\eta)^4 \\ & +\begin{pmatrix} 2.0\alpha\beta\eta_b^2\zeta_n+0.5\beta\mu\mu_d\left(\csc^2(\phi)\right)+0.5\beta\eta_b^2\mu_d\left(\csc^2(\phi)\right) \\ +\alpha\beta\eta_b^2\mu_d\zeta_n\left(\csc^2(\phi)\right)+\beta\eta_b^2+\beta+2.0\alpha\zeta_n \\ +\beta\mu_k+\alpha\mu\mu_d\zeta_n\left(\csc^2(\phi)\right)+0.5\beta\mu\mu_d\mu_k\left(\csc^2(\phi)\right) \end{pmatrix}(i\eta)^3 \\ & +\begin{pmatrix} 0.5\alpha\mu\mu_d\left(\csc^2(\phi)\right)+0.5\alpha\beta\eta_b^2\mu_d\mu_k\left(\csc^2(\phi)\right) \\ +0.5\alpha\beta\eta_b^2\mu_d\left(\csc^2(\phi)\right) \\ +\alpha\eta_b^2+1.0\alpha+\alpha\beta\eta_b^2\mu_k+\alpha\beta\eta_b^2\kappa^2 \\ +\alpha\mu_k+0.5\alpha\mu\mu_d\mu_k\left(\csc^2(\phi)\right)+\beta\eta_b^2\mu_d\zeta_n\left(\csc^2(\phi)\right) \\ +0.5\alpha\eta_b^2\mu_d\left(\csc^2(\phi)\right)+\alpha\beta\eta_b^2+2.0\beta\eta_b^2\zeta_n \end{pmatrix}(i\eta)^2 \\ & +\begin{pmatrix} 0.5\beta\eta_b^2\mu_d\mu_k\left(\csc^2(\phi)\right)+\beta\eta_b^2\mu_k+\beta\eta_b^2 \\ +\alpha\eta_b^2\mu_d\zeta_n\left(\csc^2(\phi)\right)+0.5\beta\eta_b^2\mu_d\left(\csc^2(\phi)\right)+2.0\alpha\eta_b^2\zeta_n \end{pmatrix}(i\eta) \\ & +\alpha\eta_b^2\mu_k+0.5\alpha\eta_b^2\mu_d\left(\csc^2(\phi)\right)+0.5\alpha\eta_b^2\mu_d\mu_k\left(\csc^2(\phi)\right)+\alpha\eta_b^2 \end{aligned} \tag{28}$$

From equation Eq. (27), the dynamic response and the voltage output of the system resulting from harmonic base excitation are derived as:

$$\begin{aligned} Y(i\eta) &= \frac{\left(\alpha\beta\eta^2-i\eta\beta-\alpha\right)\begin{pmatrix} 0.5\mu_d\eta_b^2\left(\csc^2(\phi)\right)-0.5\mu_d\mu\eta^2\left(\csc^2(\phi)\right) \\ +\eta_b^2-\eta^2 \end{pmatrix}}{\Delta_2(i\eta)} \times \left(\frac{Y_b}{\omega_n^2}\right) \\ \text{and} \quad V(i\eta) &= \frac{-\eta^2\alpha\beta\theta\left(0.5\mu_d\eta_b^2\left(\csc^2(\phi)\right)-0.5\mu_d\mu\eta^2\left(\csc^2(\phi)\right)+\eta_b^2-\eta^2\right)}{C_p\Delta_2(i\eta)} \times \left(\frac{Y_b}{\omega_n^2}\right) \end{aligned} \tag{29}$$

Similar to the prior case, the voltage at $\eta = 1$ with zero damping and absent the inertial amplifier is deemed suitable for normalisation.

$$V_0 = V(i\eta)|_{\{\eta=1,\zeta_n=0,\mu_d=0,\Gamma_k=0\}} = \frac{\theta}{\kappa^2 C_p}\left(\frac{Y_b}{\omega_n^2}\right) \tag{30}$$

From this, the non-dimensional voltage response is derived as:

$$\begin{aligned} \widehat{V}(i\eta) &= \frac{V(i\eta)}{V_0} \\ &= \frac{\eta^2\alpha\beta\left(-0.5\mu_d\eta_b^2\left(\csc^2(\phi)\right)+0.5\mu_d\mu\eta^2\left(\csc^2(\phi)\right)-\eta_b^2+\eta^2\right)\kappa^2}{\Delta_2(i\eta)} \end{aligned} \tag{31}$$

The non-dimensional power is derived from Eq. (31) using this expression. Subsequently, the influence of the inertial amplifier on the harvested power is examined.

The non-dimensional harvested power, derived from the voltage expression in Eq. (31), is illustrated as a function of the non-dimensional frequency in Fig. 8. Two parameter sets are evaluated for the inertial amplifier: $\mu_d = 0.2$, $\Gamma_k = 1$, $\phi = 10°$ and $\mu_d = 1$, $\Gamma_k = 1.5$, $\phi = 15°$. The non-dimensional inductor constant is assumed to be $\beta = 1.0$. Both exhibit increased harvested power at a higher frequency relative to the traditional scenario devoid of any inertial amplifier. The addition of inductance provides more harvested power compared to the non-inductance harvester but at a higher frequency. The system in Fig. 8(b) exhibits greater harvested power than the system in Fig. 8(a). The configuration shown in Fig. 8(a) (where $\mu_d = 0.2$ and $\phi = 10°$) achieves a 99.57% power enhancement compared to the traditional harvester. The maximum non-dimensional power generated by NSIA is 217.42, whereas the traditional harvester without NSIA produces a power output of 0.9334. For instance, the system depicted in Fig. 8(b), with parameters $\mu_d = 1$, and $\phi = 15°$, exhibits a power output exceeding 99.66% that of the traditional harvester at lower frequencies. The maximum non-dimensional power generated by NSIA is 282.29, whereas the traditional harvester without NSIA produces a power output of 0.9334. These results highlight the significant power enhancement achieved through NSIA, demonstrating its effectiveness in improving energy harvesting performance across different configurations. The harvester with inductance generates more energy in higher frequency regions when the negative stiffness inertial amplifier is applied. Therefore, a harvester without inductance is suitable for energy harvesting at low frequency. The maximum power output from each harvester is listed in Table 4. Fig. 9 presents the non-dimensional power spectral density (PSD) response of a harvester with an inductor ($\mu_d = 0.2$, $\Gamma_k = 1$, $\phi = 10°$ and $\mu_d = 1$, $\Gamma_k = 1.5$, $\phi = 15°$) under random excitation, comparing the performance of a classical harvester lacking an inertial amplifier (IA) and two configurations of harvesters equipped with a negative stiffness inertial amplifier (NSIA).

Table 4
Non-dimensional power under harmonic excitation.

Device	Power
NSIA ($\phi = 10°$)	217.42
NSIA ($\phi = 15°$)	282.29
Without NSIA (Conventional energy harvester)	0.9334

Performance comparison:

- Without NSIA (classical harvester): The PSD for the classical harvester is consistently lower across all frequencies. Its peak occurs near $\eta \approx 1$ (the resonance frequency), but the power output remains relatively modest due to the absence of inertial amplification or stiffness adjustment mechanisms. At higher frequencies ($\eta > 1.5$), the PSD decreases sharply, indicating diminished energy harvesting capability.
- With NSIA (proposed harvester): Harvesters featuring NSIA demonstrate significantly enhanced PSD across a wide range of frequencies. The power generated is approximately four to seven times greater than that of the classical harvester, especially near resonance ($\eta \approx 1$).

NSIA introduces dynamic negative stiffness and effectively amplifies the system's inertial mass, enabling better energy harvesting under random excitations by increasing the system's responsiveness at low frequencies. Influence of NSIA:

- Dynamic negative stiffness: The inclusion of NSIA reduces the effective stiffness of the harvester. This enables the system to achieve resonance at lower excitation frequencies ($\eta < 1$), where the classical harvester performs poorly. The sharp peaks in the PSD for NSIA configurations indicate enhanced energy absorption near these resonances.
- Dynamic mass amplification: NSIA increases the effective dynamic mass of the harvester, which amplifies its ability to extract energy from random excitations. This dynamic mass enhancement contributes to higher PSD levels across the entire frequency range, as seen in the significant separation between the "With NSIA" and "Without NSIA" curves.

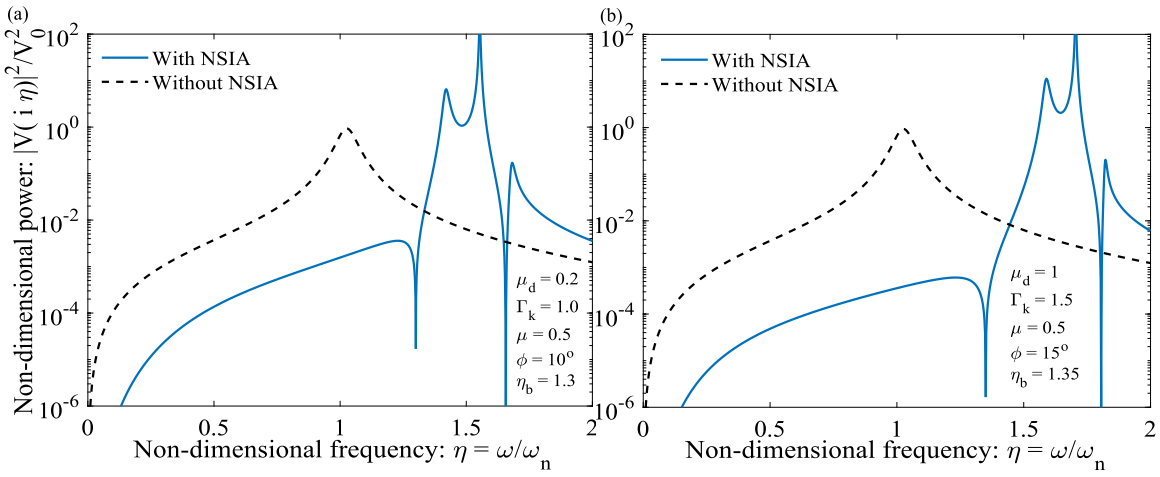

Fig. 8. The non-dimensional power of a harvester with an inductor ($\zeta = 0.011$, $\alpha = 0.8649$, $\kappa^2 = 0.1185$, $\beta = 1.0$) as a function of non-dimensional frequency. The powers acquired from the classical harvester lacking an inertial amplifier and the proposed harvester featuring two distinct inertial amplifier configurations are presented for comparison. The power generated by the proposed harvesters is approximately four to seven times greater than that of the conventional harvester.

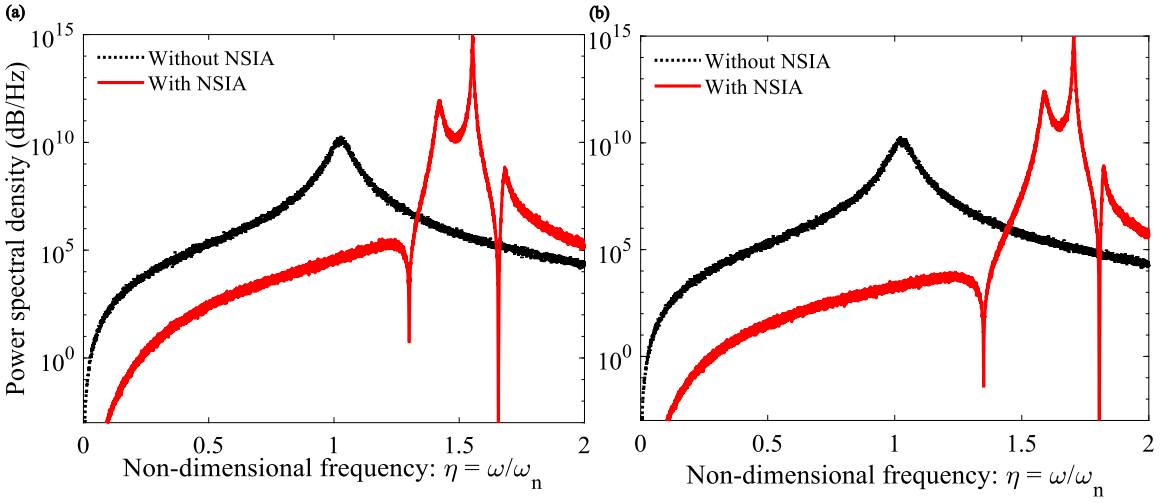

Fig. 9. The non-dimensional power spectral density (PSD) of a harvester with an inductor ($\zeta = 0.011$, $\alpha = 0.8649$, $\kappa^2 = 0.1185$, $\beta = 1.0$) under random excitation, plotted as a function of non-dimensional frequency. The PSDs acquired from the classical harvester lacking an inertial amplifier and the proposed harvester featuring two distinct inertial amplifier configurations are presented for comparison. The power generated by the proposed harvesters with NSIA is approximately four to seven times greater than that of the conventional harvester, demonstrating significant performance enhancement under random excitation.

Comparison between NSIA configurations (Fig. 9(a) and (b)):

- Configuration Fig. 9(a): This configuration corresponds to a smaller mass ratio ($\mu_d = 0.2$) and amplifier angle ($\phi = 10°$). It exhibits sharp PSD peaks near $\eta \approx 1.5$, reflecting strong resonance at higher frequencies. The PSD enhancement is significant compared to the classical harvester but slightly lower than Configuration Fig. 9(b) due to the reduced dynamic mass and less effective stiffness modulation.
- Configuration Fig. 9(b): This configuration uses a larger mass ratio ($\mu_d = 1$) and amplifier angle ($\phi = 15°$). It demonstrates sharper and higher PSD peaks across the frequency range, particularly at lower frequencies ($\eta \approx 1$). The larger mass ratio provides greater inertial amplification, allowing for better energy harvesting even under conditions of higher damping and random excitation.

Frequency behaviour:

- Resonance efficiency: For both NSIA configurations, the PSD peaks are sharper and more pronounced compared to the classical harvester, indicating superior resonance efficiency. These peaks are also broader, suggesting an extended operational frequency range for energy harvesting.
- Low-frequency harvesting: NSIA configurations significantly outperform the classical harvester at lower frequencies ($\eta < 1$). This improvement is critical for real-world applications, where ambient vibrations are often concentrated at lower frequencies.

Design implications:

- Role of NSIA: The incorporation of NSIA offers substantial improvements in power harvesting efficiency, especially under random excitation. The ability to dynamically modulate stiffness and mass makes NSIA-equipped harvesters versatile and highly effective for varying environmental conditions.
- Configuration selection: Configuration Fig. 9(b) is more suitable for applications requiring enhanced performance across a wider frequency range, while Configuration Fig. 9(a) might be preferred for scenarios focusing on higher-frequency harvesting.
- Damping optimisation: The relatively low damping factor ($\zeta = 0.011$) ensures that the benefits of NSIA are maximised. Increasing

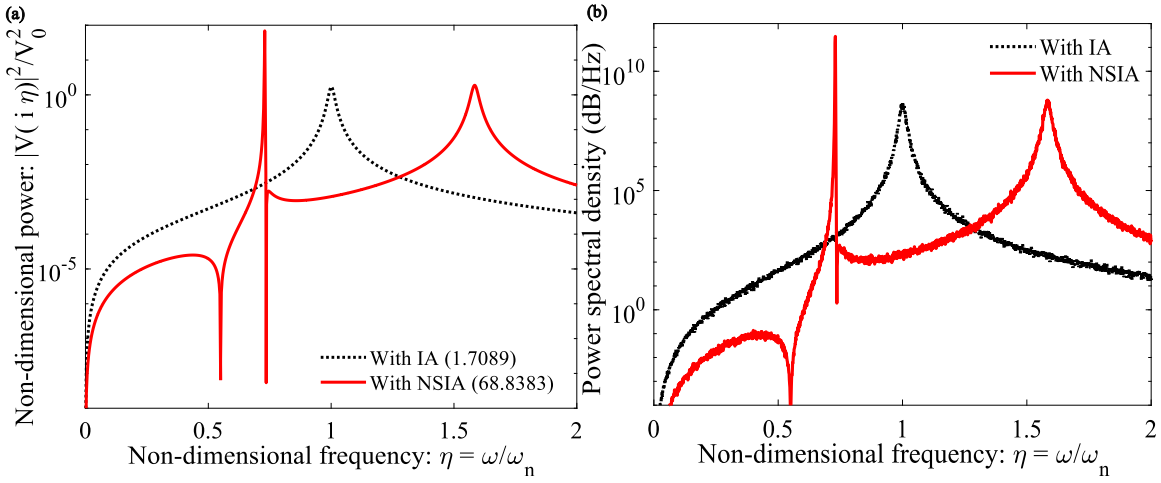

Fig. 10. Comparison of non-dimensional power output and power spectral density (PSD) as a function of non-dimensional frequency ($\eta = \omega/\omega_n$) for systems incorporating a Negative Stiffness Inertial Amplifier (NSIA) and a solely Inertial Amplifier (IA)-based harvester. (a) Non-dimensional power output under harmonic excitation shows a significant enhancement for the NSIA system, which achieves a peak power of 68.83 compared to 1.7089 for the IA system. (b) Power spectral density (PSD) under random excitation, highlighting the broader and lower-frequency resonance of the NSIA system, demonstrating its effectiveness in enhancing power harvesting from low-frequency vibrations.

Table 5
Non-dimensional power under random excitation.

Device	Power
NSIA ($\phi = 10°$)	8.9185×10^{14} dB/Hz
NSIA ($\phi = 15°$)	1.6133×10^{15} dB/Hz
Without NSIA (Conventional energy harvester)	2.2692×10^{10} dB/Hz

damping would likely reduce the overall PSD, as seen in similar analyses.

The figure demonstrates the significant advantage of NSIA over classical harvesters for energy harvesting under random excitations. The dynamic amplification of mass and reduction in stiffness through NSIA allow for substantial power gains, particularly at lower frequencies and near resonance. Configuration Fig. 9(b), with its larger mass ratio and steeper amplifier angle, achieves superior PSD performance, making it the preferred design for applications requiring efficient low-frequency vibration energy harvesting. These findings highlight the transformative potential of NSIA in advancing vibration energy harvesting technologies for sustainable energy solutions. The maximum power output from each harvester is listed in Table 5.

4. Comparative study with conventional inertial amplifier-based energy harvesters

The results presented in Fig. 10 provide a comparative analysis of vibration energy harvesting performance using a Negative Stiffness Inertial Amplifier (NSIA) versus a traditional Inertial Amplifier (IA). The non-dimensional power output in panel Fig. 10(a) highlights the significant advantage of the NSIA system under harmonic excitation. The NSIA-enhanced harvester exhibits a pronounced peak at a lower non-dimensional frequency ($\eta \approx 0.5$), achieving a peak power output of 68.83, which is substantially higher than the IA system's peak power of 1.7089 at a higher frequency ($\eta \approx 1.0$). This shift to a lower resonance frequency is attributed to the negative stiffness mechanism, which effectively reduces the system's effective stiffness, enabling energy harvesting at lower frequencies where conventional IA-based systems struggle. The broader frequency response of the NSIA system also suggests greater adaptability to variations in excitation frequency, making it more effective for real-world applications where ambient vibrations

Table 6
Non-dimensional power under harmonic excitation.

Device	Power
NSIA	68.83
IA	1.7089

Table 7
Non-dimensional power under random excitation.

Device	Power
NSIA	2.894×10^{11} dB/Hz
IA	4.5847×10^{8} dB/Hz

are often broadband and low-frequency. The maximum power output from each harvester under harmonic excitation is listed in Table 6. Panel Fig. 10(b) presents the power spectral density (PSD) response under random excitation, further confirming the superiority of NSIA in low-frequency vibration energy harvesting. The PSD of the IA-based harvester reaches a maximum value of 4.5847×10^8 dB/Hz, whereas the NSIA system achieves an extraordinary 2.8940×10^{11} dB/Hz, representing an enhancement by a factor of over 99.84%. The PSD of the IA system shows a sharp peak at $\eta \approx 1.0$, similar to its harmonic excitation response, indicating that its resonance is constrained to higher frequencies. In contrast, the NSIA system demonstrates a broader spectral response, with a major peak at lower frequencies ($\eta \approx 0.5$). This broadened response is indicative of the system's enhanced bandwidth, allowing it to efficiently harvest energy from a wider range of excitation frequencies. Additionally, the NSIA system exhibits higher PSD values at lower frequencies, reflecting its ability to leverage negative stiffness effects to increase power output under stochastic excitations. Overall, these results suggest that incorporating negative stiffness in vibration energy harvesters provides a transformative improvement in energy absorption, particularly for low-frequency applications such as structural health monitoring, wireless sensor networks, and autonomous sensing technologies. The NSIA system's ability to reduce resonance frequency, increase power output, and enhance spectral bandwidth makes it far superior to conventional IA-based designs, paving the way for more efficient, self-sustaining energy harvesting technologies. The system parameters are illustrated in Table 1. The maximum power output from each harvester under random excitation is listed in Table 7.

5. Conclusions

This study introduces the use of Negative Stiffness Inertial Amplifiers (NSIAs) in cantilever bimorph piezoelectric energy harvesters to enhance low-frequency vibration energy harvesting (VEH). Traditional piezoelectric energy harvesters (PEHs) often struggle to harness energy from low-frequency vibrations due to their intrinsic stiffness, which prevents effective resonance at lower frequencies. By integrating NSIAs, the effective stiffness is significantly reduced, and the dynamic mass of the system is amplified, allowing for enhanced energy extraction at lower operational frequencies. Two circuit configurations one without an inductor and one incorporating an inductor were analysed. The results demonstrate that NSIA-equipped harvesters can generate up to 99.97% more power than conventional systems at certain frequencies, with further performance improvements when an inductor is introduced to adjust electrical resonance. The incorporation of NSIAs presents a novel paradigm in vibration energy harvesting, shifting the resonance of PEHs towards lower frequencies and achieving significant power enhancements under both harmonic and random excitations. The findings illustrate that NSIAs provide a highly efficient and scalable solution for autonomous power generation, with applications in wireless sensor networks, structural health monitoring, and smart infrastructure. Furthermore, the comparative study with conventional inertial amplifiers (IAs) underscores the transformative role of NSIAs in VEH, with NSIAs demonstrating a nearly 99.84% increase in power output compared to traditional inertial amplifiers in low-frequency conditions. These insights pave the way for advanced energy-harvesting technologies that can efficiently operate in real-world, broadband vibration environments.

- Introduction of NSIAs: This study pioneers the use of NSIAs in piezoelectric VEH, achieving significantly enhanced power output by reducing the effective stiffness of the system.
- Optimisation of NSIA parameters: A systematic optimisation framework was developed, refining key parameters (stiffness ratio, mass ratio, amplifier angle) to maximise harvested power.
- Dual circuit configurations: Performance evaluation of both inductor-free and inductor-based circuits demonstrates how electrical tuning further enhances energy harvesting efficiency.
- Enhanced low-frequency energy harvesting: The proposed system achieves 99.97% more power generation than conventional PEHs.
- Comparative analysis with traditional Inertial Amplifiers (IAs): Demonstrated that NSIAs outperform IAs by nearly two orders of magnitude, offering a superior alternative for low-frequency vibration applications.

The findings of this study have profound implications for self-powered sensing technologies and sustainable energy solutions. By leveraging NSIAs, energy harvesters can be tuned to efficiently capture energy from ambient low-frequency vibrations, making them ideal for structural health monitoring, industrial IoT, and autonomous wireless devices. Additionally, the ability to fine-tune electrical resonance via inductors offers new design pathways for adaptive energy-harvesting systems that can dynamically adjust to varying environmental conditions. For the future scope of the research, experimental validation of the proposed NSIA-integrated energy harvester will be conducted by fabricating and testing a physical prototype. In addition, future work will focus on a detailed parametric analysis through experiments to evaluate the influence of structural parameters, such as cantilever beam dimensions and NSIA configurations, on energy harvesting efficiency for further system optimisation.

This study establishes NSIAs as a disruptive advancement in VEH, offering a scalable, efficient, and robust mechanism for maximising power generation from ambient vibrations. The work not only advances theoretical insights but also lays the foundation for next-generation energy-harvesting technologies poised to drive innovation in self-powered electronic systems.

CRediT authorship contribution statement

Sudip Chowdhury: Writing – review & editing, Writing – original draft, Visualization, Validation, Supervision, Software, Resources, Project administration, Methodology, Investigation, Funding acquisition, Formal analysis, Data curation, Conceptualization. **Sondipon Adhikari:** Writing – review & editing, Visualization, Supervision, Software, Resources, Project administration, Methodology, Conceptualization. **Arnab Banerjee:** Writing – review & editing, Supervision, Project administration, Methodology, Conceptualization.

Declaration of competing interest

The authors declare that they have no known competing financial interests or personal relationships that could have appeared to influence the work reported in this paper.

Acknowledgements

Sudip Chowdhury would like to acknowledge the Postdoctoral research grant received from The University of Glasgow for the financial support of this research.

Appendix A. List of symbols

- m: Static tip mass of the harvester.
- m_a: Amplifier mass.
- m_b: Static mass of the lateral spring-mass system.
- m_d: Total static mass of the negative stiffness inertial amplifier.
- m_{ia}: Dynamic effective mass of the amplifier.
- μ: Mass the ratio of the negative stiffness inertial amplifier.
- ω_n: Natural frequency of the harvester.
- ω: Excitation frequency.
- η: Excitation frequency ratio.
- η_b: Frequency ratio of the lateral spring-mass system.
- m_h: Dynamic effective mass of the harvester.
- ϕ: Amplifier angle.
- R_l: Load resistance for the harvesting circuit.
- c_h: Dynamic effective damping of the harvester.
- k_h: Dynamic effective stiffness of the harvester.
- k_b: Negative stiffness of the lateral spring-mass system.
- k_a: Stiffness of the negative stiffness inertial amplifier.
- Γ_k: Stiffness ratio.
- θ: Electromechanical coupling.
- Γ_h: Effective mass ratio.
- $\ddot{y}_b$: Deterministic harmonic excitation.
- ζ_n: Harvester's damping factor.
- α: Dimensionless time constant.
- C_p: Capacitance.
- L: Inductance of the circuit.
- β: Normalised inductor parameter.

Appendix B. List of abbreviations

- VEH: Vibration energy harvesting.
- NSIA: Negative stiffness inertial amplifiers.
- IA: Inertial amplifiers.
- PEH: Conventional piezoelectric energy harvesters

Data availability

All data, models, and code generated or used during the study appear in the submitted article.

References

[1] X. Yang, T. Zhang, Y. Shen, Y. Liu, V. Bui, D. Qiu, Tradeoff analysis of the energy-harvesting vehicle suspension system employing inerter element, Energy 308 (2024) 132841.

[2] Y. Cui, T. Yang, H. Luo, Z. Li, X. Jing, Jellyfish-inspired bistable piezoelectric-triboelectric hybrid generator for low-frequency vibration energy harvesting, Int. J. Mech. Sci. 279 (2024) 109523.

[3] A. Ali, S. Ali, H. Shaukat, E. Khalid, L. Behram, H. Rani, W.A. Altabey, S.A. Kouritem, M. Noori, Advancements in piezoelectric wind energy harvesting: A review, Results Eng. (2024) 101777.

[4] H. Salehi, R. Burgueño, S. Chakrabartty, N. Lajnef, A.H. Alavi, A comprehensive review of self-powered sensors in civil infrastructure: State-of-the-art and future research trends, Eng. Struct. 234 (2021) 111963.

[5] Z. Ye, X. Li, W. Tang, K. Huang, Y. Wei, F. Mo, An integrated vibration energy harvesting-storage-injection system based on piezoelectric bistable, Smart Mater. Struct. 34 (2) (2025) 025024.

[6] D.K. Khatua, S.-J. Kim, Perspective on the development of high performance flexible piezoelectric energy harvesters, J. Mater. Chem. C 10 (8) (2022) 2905–2924.

[7] R. Sun, S. Zhou, L. Cheng, Ultra-low frequency vibration energy harvesting: Mechanisms, enhancement techniques, and scaling laws, Energy Convers. Manage. 276 (2023) 116585.

[8] Q. Cai, S. Zhu, The nexus between vibration-based energy harvesting and structural vibration control: A comprehensive review, Renew. Sustain. Energy Rev. 155 (2022) 111920.

[9] V. Vallem, Y. Sargolzaeiaval, M. Ozturk, Y.-C. Lai, M.D. Dickey, Energy harvesting and storage with soft and stretchable materials, Adv. Mater. 33 (19) (2021) 2004832.

[10] P. Cao, S. Zhang, Z. Wang, K. Zhou, Damage identification using piezoelectric electromechanical impedance: a brief review from a numerical framework perspective, in: Structures, Vol. 50, Elsevier, 2023, pp. 1906–1921.

[11] T. Yang, S. Zhou, S. Fang, W. Qin, D.J. Inman, Nonlinear vibration energy harvesting and vibration suppression technologies: Designs, analysis, and applications, Appl. Phys. Rev. 8 (3) (2021).

[12] L.-C. Zhao, H.-X. Zou, K.-X. Wei, S.-X. Zhou, G. Meng, W.-M. Zhang, Mechanical intelligent energy harvesting: from methodology to applications, Adv. Energy Mater. 13 (29) (2023) 2300557.

[13] P. Yin, L. Tang, Z. Li, C. Xia, Z. Li, K.C. Aw, Harnessing ultra-low-frequency vibration energy by a rolling-swing electromagnetic energy harvester with counter-rotations, Appl. Energy 377 (2025) 124507.

[14] D. Pan, Y. Liang, Z. Zhang, Z. Wu, Design and dynamics of a cantilevered bistable buckled piezoelectric beam for vibrational energy harvesting, Mech. Syst. Signal Process. 224 (2025) 112013.

[15] H. Tang, C. Hua, H. Huang, W. Liu, Z. Yang, Y. Yuan, Z. Zhang, Low-frequency vibration energy harvesting: a comprehensive review of frequency up-conversion approaches, Smart Mater. Struct. 31 (10) (2022) 103001.

[16] H. Wu, Z. Zhu, J. Li, J. Xu, A novel electromagnetic energy harvester by elastic oscillating, Mech. Syst. Signal Process. 225 (2025) 112329.

[17] M.O. Awadallah, C. Jiang, O. el Moctar, A.A. Hassan, Boosting energy harvesting efficiency from wake-induced vibration using a multi-cylinder configuration, Appl. Energy 381 (2025) 125181.

[18] J. Chen, J. Liu, B. Bao, Dual-source energy harvester for collecting both flow-induced and multi-directional vibratory energies, Nonlinear Dynam. 113 (4) (2025) 3119–3146.

[19] W. Zhou, D. Du, Q. Cui, C. Lu, Y. Wang, Q. He, Recent research progress in piezoelectric vibration energy harvesting technology, Energies 15 (3) (2022) 947.

[20] W. Zhou, D. Du, Q. Cui, Z. Yang, C. Lu, Y. Wang, Q. He, Piezoelectric vibration energy harvester: Operating mode, excitation type and dynamics, Adv. Mech. Eng. 14 (10) (2022) 16878132221131177.

[21] B. Zhao, T.-B. Xu, Finite element modelling and experimental validations of proof mass effects on flextensional piezoelectric energy harvesters, Sensors Actuators A: Phys. 383 (2025) 116185.

[22] H. Jing, H. Xiang, J. Wang, Modified vortex-induced vibration piezoelectric energy harvester for capturing wind energy from trains moving in tunnels, Sensors Actuators A: Phys. 382 (2025) 116136.

[23] H. Djellal, B. Morrone, L. Costanzo, M. Vitelli, A. Saad, Parametric study of a ball-screw energy harvester shock absorber, in: E3S Web of Conferences, Vol. 602, EDP Sciences, 2025, p. 01007.

[24] X. Wang, X. Kang, W. Zhu, Z. Zhu, C. Wang, Nonlinear vibration and energy harvesting analysis of a quasi-zero stiffness system with an inertial amplifier, J. Vib. Eng. Technol. 13 (1) (2025) 1–19.

[25] H. Liang, G. Hao, O.Z. Olszewski, A review on vibration-based piezoelectric energy harvesting from the aspect of compliant mechanisms, Sensors Actuators A: Phys. 331 (2021) 112743.

[26] J. Fang, B. Hu, M. Jiang, C. Li, M. Lv, A piezoelectric-electromagnetic hybrid energy harvester for low-frequency impact vibration, J. Magn. Magn. Mater. 614 (2025) 172761.

[27] X. Huang, B. Wang, Z. Huang, X. Hua, Z. Chen, A theoretical model for a low-frequency two-stage hybrid vibration isolator with a nonlinear energy sink and a negative stiffness spring, Appl. Math. Model. (2025) 115948.

[28] H. Alimohammadi, K. Vassiljeva, S.H. HosseinNia, E. Petlenkov, Nonlinear dynamics in PEH for enhanced power output and vibration suppression in metastructures, Nonlinear Dynam. (2024) 1–23.

[29] M. Wu, R. Gao, Y. Zhou, J. Che, J. Wu, X. Li, X. Chen, W. Jiang, Analysis and experiment of a multi-tile magnetic spring with high negative stiffness, Mech. Syst. Signal Process. 223 (2025) 111914.

[30] D. Tan, X. Ou, J. Zhou, K. Wang, H. Pan, J. Peng, H. Sun, Magnetic tri-stable triboelectric nanogenerator for harvesting energy from low-frequency vibration, Renew. Energy (2025) 122517.

[31] X. Huang, X. Hua, Z. Chen, Exploiting a novel magnetoelastic tunable bi-stable energy converter for vibration energy mitigation, Nonlinear Dynam. 113 (3) (2025) 2017–2043.

[32] X. Wang, X. Kang, L. Ji, A. Zhang, G. Xia, Low frequency vibration energy harvesting of bio-inspired multi-stable piezoelectric vibration system with an adjustable device, Chaos Solitons Fractals 192 (2025) 116026.

[33] N. Almarri, J. Chang, W. Song, D. Jiang, A. Demosthenous, Piezoelectric energy harvesting and ultra-low-power management circuits for medical devices, Nano Energy (2024) 110196.

[34] Z. Yang, Y. Zhang, Z. Li, S. Lin, Y. Gu, W. Liao, Z. Zhang, J. Kan, Design and characterization of a wind-adaptable piezoelectric energy harvester utilizing a rigid-flexible compound blunt body, Mech. Syst. Signal Process. 223 (2025) 111913.

[35] J. Luo, L. Zhang, L. Miao, Y. Mao, A new magnetic negative stiffness mechanism: A case study of fast steering mirror for quasi-zero stiffness vibration isolation, Adv. Mech. Eng. 16 (10) (2024) 16878132241288091.

[36] J. Ghazanfarian, M.M. Mohammadi, K. Uchino, Piezoelectric energy harvesting: a systematic review of reviews, in: Actuators, Vol. 10, MDPI, 2021, p. 312.

[37] B. Lafarge, S. Grondel, C. Delebarre, O. Curea, C. Richard, Linear electromagnetic energy harvester system embedded on a vehicle suspension: From modeling to performance analysis, Energy 225 (2021) 119991.

[38] S. Chowdhury, A. Banerjee, S. Adhikari, Optimal negative stiffness inertial-amplifier-base-isolators: exact closed-form expressions, Int. J. Mech. Sci. 218 (2022) 107044.

[39] Z. Zhao, Q. Chen, R. Zhang, C. Pan, Y. Jiang, Energy dissipation mechanism of inerter systems, Int. J. Mech. Sci. 184 (2020) 105845.

[40] S. Ali, M. Friswell, S. Adhikari, Piezoelectric energy harvesting with parametric uncertainty, Smart Mater. Struct. 19 (10) (2010) 105010.